Dynamic Characterization of Noise and Vibration Transmission Paths in Linear Cyclic Systems (II)

- Experimental Validation -

Han Jun Kim
1531 13th Street, Columbus, Indiana 47201, U. S. A.
Young Man Cho*
School of Mechanical and Aerospace Engineering, Seoul National University

Linear cyclic systems (LCS's) are a class of systems whose dynamic behavior changes periodically. Such a cyclic behavior is ubiquitous in systems with fundamentally repetitive motion. Yet, the knowledge of the noise and vibration transmission paths in LCS's is quite limited due to the time-varying nature of their dynamics. The first part of this two-part paper derives a generic expression that describes how the noise and/or vibration are transmitted between two (or multiple) points in the LCS's. In Part II, experimental validation of the theoretical development of Part I is provided. The noise and vibration transmission paths of the scroll and rotary compressors (two typical LCS's) are examined to show that the LCS's indeed generate a series of amplitude modulated input signals at the output, where the carrier frequencies are harmonic multiples of the LCS' fundamental frequency. The criterion proposed in Part I to determine how well a given LCS can be approximated as a linear time-invariant systems (LTIS) is applied to the noise and vibration transmission paths of the two compressors. Furthermore, the implications of the experimental validations/applications are discussed in order to assess the applicability of the noise/vibration source and transmission path identification techniques based on the assumption that the system under consideration is linear and time-invariant.

Key Words : Linear Cyclic System, Rotary Compressor, Scroll Compressor

1. Introduction

It has become an overwhelming industry trend to eliminate or reduce the noise and vibration from dynamic systems through various means such as product redesign, passive damping, active control of noise and vibration, etc. (Faulker, 1976 ; Comparin, 1994 ; Bradley, 1993 ; Smith et al., 1992 ; Ha, 1995 ; Oh, 1993). The noise and vibration reduction/control is particularly important for systems irderacting with the use, even though its importance for non-residential counterparts is equally recognized. It is unthinkable nowadays to place in the market a final product that generates an unpleasant level of noise/vibration. The first step toward the noise/vibration reduction is to understand the mechanism(s) of the noise/vibration generation and transmission and then to locate the noise/vibration sources and transmission paths. Numerous papers have dealt with these issues (Tamaki et al., 1995 ; Barker and Hinich, 1994 ; Harrap and Wang, 1994 ; Cann, 1992 ; Meng and Qu 1991 ; Young, 1994 ; Lou et al., 1993 ; Rantala and Suoranta, 1991 ; Kinsler et al., 1982 ; Belousov and Rimskii -Korsakov, 1975 ; Ten Wolde, 1973 ; Ten Wolde, 1976) and have been quite successful in identify-

* Corresponding Author,
E-mail : choym@gong.snu.ac.kr
TEL : +82-2-880-1694 ; **FAX** : +82-2-883-1513
School of Mechanical and Aerospace Engineering, Seoul National University San 56-1, Shilim-dong, Kwanak-gu, Seoul, 151-742, Korea (Manuscript **Received** December 16, 1999; **Revised** June 24, 2000)

ing the noise/vibration sources and transmission paths. However, they all fail to discuss the interaction between the noise/vibration sources and transmission paths. It is interesting to note that these papers are devoted to two different classes of dynamic systems without detailed discussions on the classification of the dynamic systems treated: linear time-invariant systems (LTIS's) and/or general (linear or nonlinear, time-varying or time-invariant) dynamics systems (GDS's). In practice, the classification of the dynamic systems into the LTIS's or GDS's is not a trivial task. For a subclass of the GDS's the linear cyclic systems (LCS's), Part I of this two-part paper derives 1) a generic expression describing the interaction between the sources and transmission paths, and 2) a criterion used to classify a given LCS into a genuine linear cyclic system (GLCS) or a pseudo linear cyclic system (PLCS)/LTIS.

In Part II, the theoretical developments derived in Part I are validated with experimental results on a couple of cyclic systems, the scroll and rotary compressors. These two compressors are widely used in residential air-conditioning units and their noise/vibration characteristics have been playing significant roles as a market discriminator, which has made it a common practice on the product design stage to check that the noise/vibration level of the compressor is under a pre-determined critical value. In Part II, the noise/vibration sources and their interactions with the transmission paths in the two compressors are understood within the framework of the theoretical developments of Part I. The compressor dynamics of interest must be linear and cyclic for the theory in Part I to be applicable to the compressors. It is the noise/vibration transmission paths of the compressor dynamics that attract our attention. Even though the fundamental mechanisms of generating noise/vibration are nonlinear, the transmission paths of the compressors can well be approximated as linear and cyclic in that 1) the noise/vibration sources are defined as nonlinear phenomena such as impact, gas discharge, etc., 2) the transmission paths themselves consist of rigid bodies, and 3) the compressor motions are approximately synchronized with the 60 Hz power line. Once the basic LCS assumptions on the transmission paths are satisfied, the predictions made on the LCS's in Part I are verified with experimental data. The two compressors are shown to produce amplitude modulated input signals at the output points along the reverse path that is used in the reciprocity experiment (Kinsler et al., 1982 ; Belousov and Rimskii-Korsakov, 1975 ; Ten Wolde, 1973 ; Ten Wolde, 1976). In addition, the experimental results support the claim in Part I that the phases of the sideband signals are not synchronous with that of the output signal at the excitation frequency and are related to the angular position (so-called the abstract angle 'θ' in Part I of the compressor) at the instant of excitation. The sideband criterion is applied in order to classify the two compressors as either a GLCS or a PLCS. The result shows that both compressors are the PLCS's and hence essentially the LTIS's. The implications of the classifications on signal processing techniques for the noise/vibration sources and transmission paths are briefly discussed.

Section 2 presents experimental validation with a scroll compressor. Various theoretical developments in Part I are verified, and the scroll compressor is classified as a PLCS. Section 3 follows the outline of Sec. 2 but describes the experimental validation with a rotary compressor. The rotary compressor is also classified as a PLCS. The purposes of the experiments and analyses in Sec. 2 and 3 are three-fold:

1. An LCS produces amplitude modulated input signals at the output.
2. The phases of the sideband signals are dependent upon the angular position of an LCS.
3. The sideband criterion is applied to classify the two compressors into either a PLCS or GLCS.

2. Experimental Validation with a Scroll Compressor

In this section, the analysis in Part I of this paper is validated with experimental data

obtained from a scroll compressor. The scroll compressor is increasingly used for a residential air-conditioning unit due to its higher efficiency compared with other compressors. The tested scroll compressor is plugged into the 60Hz power line and is driven by an AC motor which is synchronized with the power line[1]. As a result, the mechanical vibration and the acoustic radiation from the compressor are synchronized with the motor speed and consist of the harmonics of the motor speed.

The scroll compressor is instrumented both internally and externally (total of two sensors) as shown in Fig. 1. The internal sensor is located near the Oldham coupling and the external one is placed on the shell. The internal transducer 'A' is an accelerometer measuring mechanical vibration in the compressor. The internal transducer measures both the induced vibration (by the external force transducer) and intrinsic vibration (by the running compressor). The external transducer 'B' is a force transducer measuring the applied force. A sinusoid is chosen as the forcing function (or waveform) in order to take advantage of a frequency domain experiment as explained in Section 5, Part I of this two-part paper. The HP spectrum analyzer is used throughout the experiment to 1) generate the forcing function, 2) collect the sensor readings, and 3) record the measured data. In the following discussion, the external force transducer is assumed to be the input transducer and the internal accelerometer is assumed to be the output transducer since the vibration due to the force is transmitted from the outside to inside through the running compressor, even if the compressor generated vibration is transmitted from the inside to outside. The reverse path is of primary concern for the experimental validation. Multiple sets of experiments are conducted with different excitation frequencies at the external force transducer. In this paper, only three representative sets are presented and discussed in detail, which turn out to be sufficient for experimental validation and classification based on the sideband criterion. It is worth mentioning that the vibration on the shell of the experimental scroll compressor is most active at the corresponding three frequencies of the three data sets presented here. A time series of each transducer measurement is recorded at the sampling frequency of 32.768 kHz. Each record is 40,960 samples long. The data are collected at a high sample rate and simultaneously for a long time interval so that each data set provides enough information required for the subsequent analysis. It may seem that the sample rate and data length are chosen excessively high and long. However, the data sets collected in this manner turn out to provide much more flexibility. With a set of comprehensive experimental data at hand, all the necessary treatments can be performed through the software via various signal processing techniques to meet the specific requirements rather than that the whole experiments are multiply conducted for the same operating condition and sensor locations.

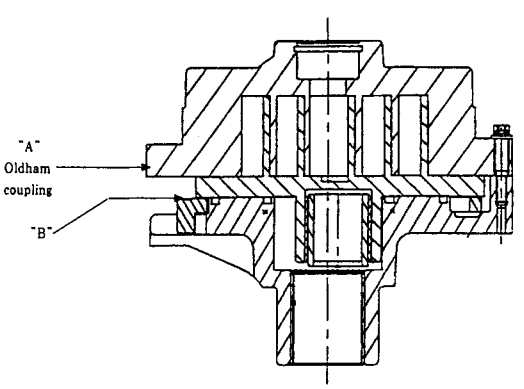

Fig. 1 The scroll compressor instrumentation diagram

Figure 2 shows a snapshot of the input/output

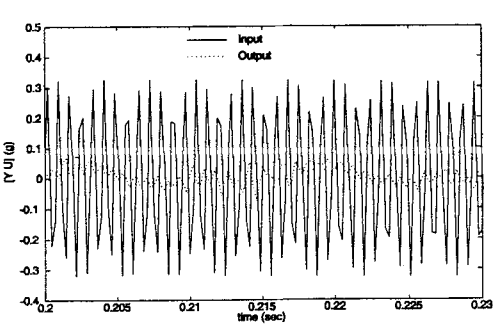

Fig. 2 A snapshot of input and output time series. The excitation frequency is 1262 Hz

[1] In fact, the motor revolution cycle slightly lags behind the cycle of the power line due to slip.

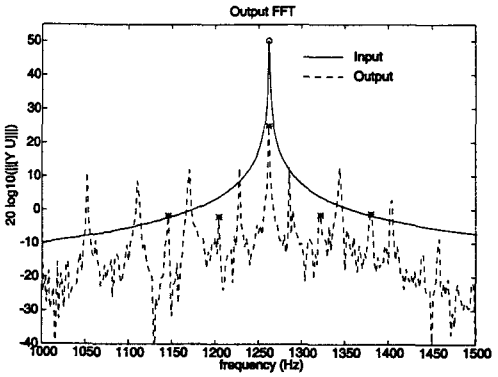

Fig. 3 The magnitude response of the input and output time series. The excitation frequency is 1262 Hz

time ser ies. The input signal is close to a pure sinusoid and the output signal contains various harmonics. This is manifested in Fig. 3, where the input/output frequency spectra are shown. The input frequency spectrum contains only one sinusoid, while the output frequency spectrum shows the various harmonics of the compressor fundamental frequency and the harmonics of the input excitation that are marked with '*' in Fig. 3. The amplitude of the input sinusoid is chosen such that either the response at the output contain enough contribution from the input transducer or a sufficient signal-to-noise ratio is attained. Note that the experimentation is conducted with the compressor running (as it should be in order to analyze the transmission paths of the running compressor) and, as a result, the intrinsic vibration measurement due to the running compressor is significant as seen in Fig. 3.

The first experiment is conducted with the sinusoid forcing at 1262 Hz. The data are prefiltered and then subsampled at a 4096 Hz. The subsampled waveform is subsequently truncated to give a 2048 sample long snapshot, starting at those time instants when the input sinusoid crosses zero positively or changes sign from negative to positive. The total of four snapshots are obtained from the subsampled waveform. The zero-crossing points are chosen to guarantee the identical phase for the input sinusoid from different snapshots. Then, any phase change in the sideband amplitude $A_k(f, t_0)$ can be traced back

Table 1(a) The magnitudes and phase angles of four different input snapshots at 1262 Hz. Each contains 2048 samples at the sampling frequency 4096 Hz

Snapshot	1	2	3	4
Magnitude	322	322	322	322
Phase Angle	−64.3	−64.4	−64.5	−64.7

Table 1(b) The magnitude response of four corresponding outputs at five different harmonic frequencies

Frequency/Snapshot	1	2	3	4
1146	0.816	0.714	0.873	0.895
1204	0.78	1.00	0.659	0.945
1262	17.5	17.6	17.6	17.5
1322	0.841	0.518	0.331	0.597
1380	0.866	0.790	0.800	1.01

Table 1(c) The corresponding phase responses

Frequency/Snapshot	1	2	3	4
1146	−42.9	117	98.8	77.2
1204	148	59.5	−140	30.9
1262	67.9	67.8	68.2	67.8
1322	−128	−38.7	140.3	−72.8
1380	129	−35.4	−18.5	17.7

to the different crankcase angle of the running compressor (as predicted in Section 3 of Part I). Table 1 and Fig. 4 show the magnitudes and phases of the input and output measurements at (the excitation frequency $\pm$ the harmonic multiples of the compressor fundamental frequency), where only significant terms are shown. The magnitude and the phase of the input signal do not change much as expected, since each snapshot is chosen to start at its positive zero-crossing instant. The slight discrepancy in the input phases is due to the finite duration effect of FFT (in other words, the length of the input signal is not infinite). A_k *at* $k=-2,\cdots,2$ is shown for each snapshot. Note that the frequencies are separated by roughly 60 Hz, which is the rotation speed of

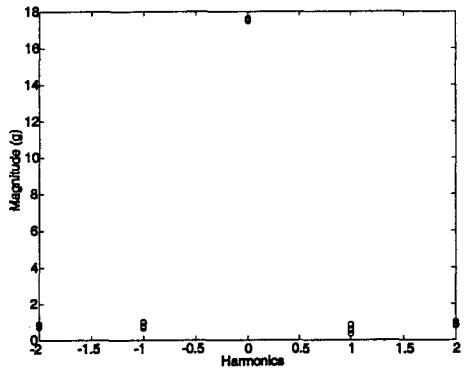

(a)

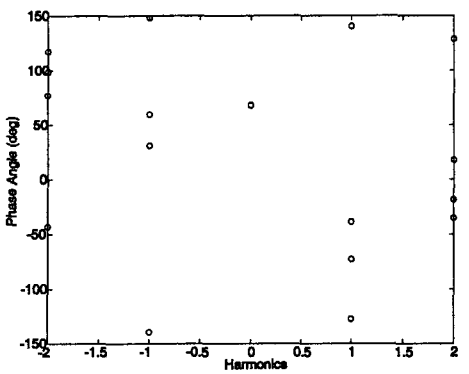

(b)

Fig. 4 (a) Magnitude response (b) Phase response. The excitation frequency is 1262 Hz

the compressor. In fact, it is slightly less than 60 Hz, which is due to slip. The amplitude modulated input signals are clearly observed at the output (the accelerometer 'A'), which verifies the prediction made in Part I. The carrier frequencies are the harmonic multiples of the rotation speed of the compressor. As also predicted by the theoretical discussion in Part I, neither the magnitudes nor the phases of the harmonics change much at the excitation frequency A_0 (1262). On the other hand, the phases of A_k *at* $k \neq 0$ change significantly from snapshot to snapshot. This is due to the different crank angles for different snapshots.

To further validate the theory developed in Part I, the same experiments are conducted at two different frequencies, 2598 Hz and 3773 Hz. Again the amplitudes of the input signals are adjusted to ensure enough signal-to-noise ratio for the input excitation. Similar analyses are

Table 2(a) The magnitudes and phase angles of four different input snapshots at 2598 Hz. Each contains 2048 samples at the sampling frequency 6554 Hz

Snapshot	1	2	3	4
Magnitude	198	198	197	197
Phase Angle	145	145	145	145

Table 2(b) The magnitude response of four corresponding outputs at five different harmonic frequencies

Frequency/Snapshot	1	2	3	4
2483	6.28	6.53	7.39	7.79
2541	4.71	4.58	4.35	4.92
2598	31.9	31.9	31.3	31.6
2659	2.02	2.06	1.62	2.14
2717	0.951	0.387	0.228	0.677

Table 2(c) The corresponding phase responses

Frequency/Snapshot	1	2	3	4
2483	−162	39.1	47.6	−99.6
2541	−74.1	24.2	−141	−40.2
2598	−42.2	−42.8	−41.7	−42.2
2659	−171	102	−102	167
2717	150	−72.3	−87.4	110

carried out for the these two experiments. The results are shown in Tables 2 and 3, Figures 5 and 6. Similar conclusions can be drawn from these figures to those of the experiment at 1262 Hz. The first two goals of the experimental validation are fulfilled.

Now the sideband criterion is applied to classify the scroll compressor. The sideband criterion states that the system under consideration is a PLCS if the following condition is satisfied: for the sideband amplitude response $A_k(f)$.

$$\int_{-\infty}^{\infty} [\sum_{k \neq 0} |A_k(f)|^2] df < \rho \alpha \int_{-\infty}^{\infty} \sum_{k=-\infty}^{\infty} |A_k(f)|^2 df \quad (1)$$

where the risk factor ρ is included in Eq. (22) of Part I. The frequency range of interest is 0-6

Table 3(a) The magnitudes and phase angles of four different input snapshots at 3773 Hz. Each contains 8192 samples at the sampling frequency 10,923 Hz

Snapshot	1	2	3	4
Magnitude	1020	1020	1020	1020
Phase Angle	155	155	156	156

Table 3(b) The magnitude response of four corresponding outputs at five different harmonic frequencies

Frequency/Snapshot	1	2	3	4
3657	44.2	43.4	43.3	43.8
3716	6.01	5.26	4.23	4.41
3773	172	171	171	171
3832	7.93	8.74	9.74	8.70
3893	3.77	4.54	3.34	4.33

Table 3(c) The corresponding phase responses

Frequency/Snapshot	1	2	3	4
3657	66.1	−10.5	−85.7	−23.2
3716	153	125	92.6	110
3773	165	166	166	116
3832	−153	−112	76.8	−104
3893	−116	21.7	−173	−75.5

kHz, where most of the vibration energy is concentrated. Then, it would be ideal for the application of the sideband criterion if the swept-sine test data (as outlined in Section 5 of Part I) are available. Multiple sets of swept-sine data were indeed collected. However, a different approach is taken here for simplicity, noting that a smaller number of frequency points can be used for certain LCS's. The sideband criterion can be evaluated with only several frequency points as long as they are representative of the whole frequency band of interest in terms of the relative sideband energy compared to the response signal energy at the excitation frequency. A careful examination of the swept-sine test data reveals that the scroll compressor belongs to such a class of LCS's and

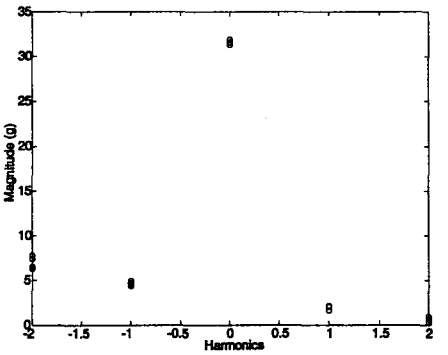

(a)

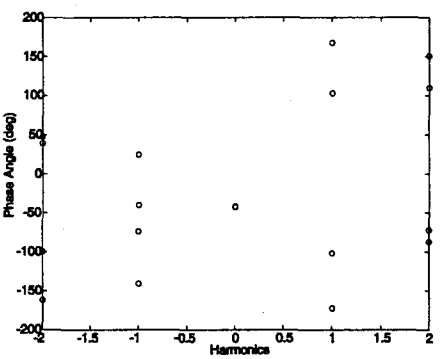

(b)

Fig. 5 (a) Magnitude response (b) Phase response. The excitation frequency is 2598 Hz

thereby makes it possible to evaluate the sideband criterion with only three frequency points 1262, 2598, 3773. Now, we approximate Eq. (1) of Part I for the selected three frequency points using $A_k(f)$ estimates in Table 1(b), Table 2(b) and Table 3(b). The critical number α and the risk factor are chosen to be 0.2 (or 7 dB) and 1.5, respectively. The $A_k(f)$ estimates from the tables must be normalized with the corresponding input amplitudes in Table 1(a), Table 2(a) and Table 3(a) before Eq. (1) is evaluated. Only $A_k(f)$ estimates of the first snapshot in each table are used.

$$
\begin{aligned}
(LHS) &= \int_{-\infty}^{\infty} [\sum_{k\neq 0} |A_k(f)|^2] df \\
&\approx [\sum_{k\neq 0} |A_k(1262)|]^2 + [\sum_{k\neq 0} |A_k(2598)|]^2 \\
&\quad + [\sum_{k\neq 0} |A_k(3773)|]^2 \\
&= 1.05 \cdot 10^{-4} + 4.97 \cdot 10^{-3} + 3.68 \cdot 10^{-3} \\
&= 8.76 \cdot 10^{-3}
\end{aligned}
$$

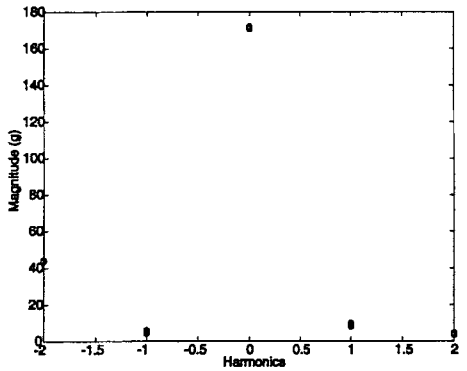

(a)

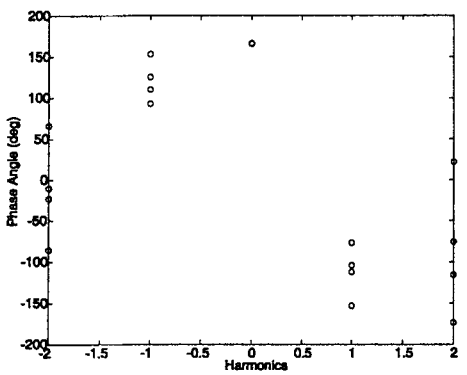

(b)

Fig. 6 (a) Magnitude response (b) Phase response. The excitation frequency is 3773 Hz

$$(RHS) = 1.5\alpha \int_{-\infty}^{\infty} \sum_{k=\infty}^{\infty} |A_k(f)|^2 df$$

$$\approx 1.5\alpha \left(\sum_{k=-2}^{2} |A_k(1262)|^2 + \sum_{k=-2}^{2} |A_k(2598)|^2 + \sum_{k=-2}^{2} |A_k(3773)|^2 \right)$$

$$= 1.5 \cdot 0.2 \cdot (2.98 \cdot 10^{-3} + 2.77 \cdot 10^{-2} + 3.01 \cdot 10^{-2}) = 1.82 \cdot 10^{-2}$$

$$\Rightarrow (LHS) < (RHS)$$

As a result, we can conclude that the scroll compressor is a PLCS/LTIS with the critical value of 0.2. The variation energy of the impulse response is less than 20% of its average energy, which indicates that the transmission paths of the scroll compressor should be close to that of a fixed structure rather than a rotating machine. Although seemingly counter-intuitive, a careful examination of the transmission paths of the scroll compressor suggests that the conclusion based on the sideband criterion makes sense. Since there exists no true rotating part in the scroll compressor other than orbiting parts, the noise/vibration transmission paths through the compressor may be approximated by a fixed structure.

Before proceeding, we examine two types of transfer functions of the noise/vibration transmission paths in the scroll compressor: the static transfer function and the dynamic one. The static transfer function is defined for the non-running compressor, while the dynamic transfer function is defined for the running compressor[2]. Both transfer functions are dependent upon the crank angle θ even though the extent of the dependence may be different. As has been verified, the dynamic transfer function does not depend heavily upon θ. On the other hand, the static transfer function depends heavily upon the crank angle, which is shown by multiple sets of experiments conducted by varying θ. The experiments indicate that the static transfer function for different θ's tends to be significantly different. Then it is natural to ask why the static transfer function is θ-dependent to such a great extent, while the dynamic transfer function is not. It is conjectured that the discrepancy between the static and dynamic transfer functions arises from the different structures along which the noise/vibration is transmitted. In the dynamic case, the noise/vibration is transmitted through a time-varying structure (still θ-dependent) which may result in a time-invariant structure on the average. In the static case, such an averaging effect cannot occur. Finally, we may as well mention that the θ-dependence of the transfer function has motivated the work presented here.

Now that the scroll compressor is classified as a PLCS/LTIS, the signal processing techniques for the LTIS's are viable tools for the compressor noise/vibration analysis. Two signal processing

[2] Of course, the dynamic transfer function is of our interest as far as the noise/vibration source and transmission path identification is concerned. However, it is not only intellectually stimulating but also beneficial to our understanding of the dynamic transfer function to examine both transfer functions simultaneously

techniques have been considered for this purpose: reciprocity experiment and system identification (Wagner and Peracchio, 1996). Both techniques were successful in identifying the noise/vibration sources and transmission paths.

3. Experimental Validation with a Rotary Compressor

This section validates the analysis in Part I with experimental data collected from a rotary compressor. The rotary compressor has been widely used in a household room air-conditioner due to its low cost and relatively high efficiency. The rotary compressor is plugged into a 60 Hz power line and is driven by an AC motor synchronized with the power line. As in the case of the scroll compressor, the compressor noise and vibration is synchronized with the motor speed. The experiments are conducted to verify the predictions based on the theoretical development in Part I and to classify the rotary compressor as either a GLCS or a PLCS.

The rotary compressor is also instrumented both internally (one sensor) and externally (one sensor) as shown in Fig. 7. The external transducer (a force transducer) is located 1 cm up vertically from the base of the compressor and horizontally 5 cm from the suction pipe. The internal transducer (an accelerometer) is at the opposite side of the compressor. The internal transducer measures vibration due to both the external force transducer and the running compressor. For the purpose of instrumentation, the compressor is not welded but bolted, which may affect the transmission path dynamics. The experimental equipment and the scheme described in Sec. 2 are adopted here and hence, they are not explained in detail here except to highlight the difference. The frequency range of interest in the rotary compressor experiment is 4500-6000 Hz, which represents the predominant vibration mode of the rotary compressor. Although multiple sets of experiments are conducted, only two of them are described here when the compressor is excited at 5060 Hz and 5460 Hz. A time series of each transducer is recorded at 16384 Hz to give a total of 60416 data points. Neither prefiltering nor subsampling is performed to the experimental data even at the signal processing level. Remember that the scroll compressor data are prefiltered and subsampled (Sec. 2). The input/output snapshots are very similar to the one shown in Figures 2 and 3 and are not shown here.

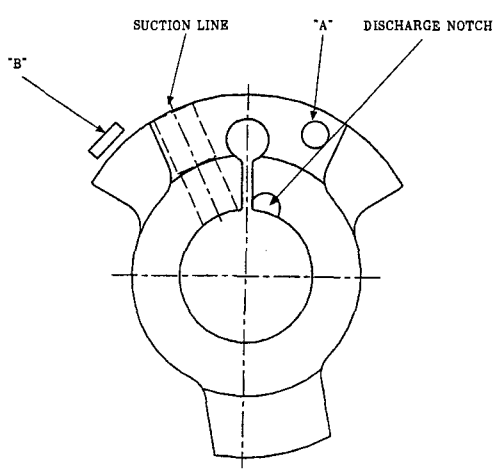

Fig. 7 The rotary compressor instrumentation diagram

The experimental data are truncated to give four 8192 sample long snapshots, starting at those

Table 4(a) The magnitude responses of four output snapshots at five different harmonic frequencies

Frequency/Snapshot	1	2	3	4
4994	40.8	33.2	35.9	46.6
5002	22.8	19.7	24.2	23.5
5060	510	513	498	501
5118	22.8	28.0	20.0	25.4
5176	18.6	22.6	22.9	15.7

Table 4(b) The corresponding phase responses

Frequency/Snapshot	1	2	3	4
4994	109	128	−161	28.6
5002	−5.5	13.5	55.0	168
5060	170	172	170	172
5118	89.0	91.3	41.0	−99.5
5176	169	153	136	−32.4

Table 5(a) The magnitude responses of four output snapshots at five different harmonic frequencies

Frequency/Snapshot	1	2	3	4
5334	19.2	18.8	17.3	1837
5402	8.21	6.78	4.95	6.04
5460	435	434	431	433
5518	30.5	29.8	32.1	29.8
5576	13.5	16.2	15.6	17.7

Table 5(b) The corresponding phase responses

Frequency/Snapshot	1	2	3	4
5344	−111	−170	176	140
5402	156	119	100	90.7
5460	111	110	110	110
5518	−124	−90.2	−76.8	−61.4
5576	−19.2	40.0	53.9	88.6

time instants when the input sinusoid crosses zero positively. Tables 4 and 5 show the magnitudes and phases of only significant sideband signals at the output. It is clear that the amplitude modulated input signals are observed at the output (the accelerometer 'A'). The magnitudes of the harmonics $A_k(f)$ do not vary much from one snapshot to the next, while the phases do vary randomly except for the phases of the harmonic signals at the excitation frequency which is constant.

Now the sideband criterion is applied to classify the rotary compressor. The frequency range of interest is 4.5-6kHz, where most of the vibration energy is concentrated. As in the case of the scroll compressor in Section 2, the sideband criterion is evaluated with only a few frequency points, 5060 and 5460, to be precise. Now, we approximate Eq. (1) for the selected two frequency points using $A_k(f)$ estimates in Table 4 (a), and Table 5(a). The critical number α and the risk factor are chosen to be 0.2 (or 7 dB) and 1.5, respectively. The $A_k(f)$ estimates from the tables are pre-normalized with the corresponding input amplitudes so that Eq. (1) can be directly evaluated without further normalization. Only $A_k(f)$ estimates of the first snapshot in each table are used.

$$
\begin{aligned}
(LHS) &= \int_{-\infty}^{\infty} [\sum_{k\neq 0} |A_k(f)|^2] df \\
&\approx [\sum_{k\neq 0} |A_k(5060)|]^2 + [\sum_{k\neq 0} |A_k(5460)|]^2 \\
&= 1.10 \cdot 10^4 + 5.09 \cdot 10^3 = 1.61 \cdot 10^4 \\
(RHS) &= 1.5\alpha \int_{-\infty}^{\infty} \sum_{k=-\infty}^{\infty} |A_k(f)|^2 df \\
&\approx 1.5\alpha \left(\sum_{k=-2}^{2} |A_k(5060)|^2 + \sum_{k=-2}^{2} |A_k(5460)|^2 \right) \\
&= 1.5 \cdot 0.2 \cdot (2.73 \cdot 10^5 + 1.91 \cdot 10^5) \\
&= 1.39 \cdot 10^5 \\
&\Rightarrow (LHS) < (RHS)
\end{aligned}
$$

The comparison between the scroll compressor and the rotary compressor discloses interesting similarities and differences in their noise/vibration transmission path dynamics. They are similar in that 1) both of them exhibit the characteristics of the LCS's such as the amplitude modulation effect, randomness of the sideband signal phases, etc. , and 2) both of them can be classified as the PLCS's, which is verified by the sideband criterion. Roughly speaking, the similarities in their responses can be traced to their structural similarity (rotating parts within a rigid body). The most conspicuous difference is the level of sideband signals, which also leads to the different ratios between the variation energy and the average energy. In Section 2, the application of the sideband criterion shows that the ratio between the variation energy and the average energy is $9.62 \cdot 10^{-2} (= 8.76 \cdot 10^{-3} / 9.11 \cdot 10^{-2})$, in which the risk factor has been included. On the other hand, the corresponding ratio of the rotary compressor is $2.31 \cdot 10^{-2} (= 1.61 \cdot 10^4 / 6.96 \cdot 10^5)$, in which the risk factor has been also included. The above analysis shows that the transmission path(s) of the scroll compressor varies more as a function of the crankcase angle θ than that of the rotary compressor. A careful comparison between the compressor structures reveals the following two causes that may contribute to such a significant discrepancy.

(1) Figure 1 shows that the scroll compressor has a direct noise/vibration transmission path between (or across, to be precise) the internal and

external transducers since the fixed scroll and the orbiting scroll are always in contact with each other in addition to the indirect path around the compressor shell. On the contrary, Fig. 7 shows that there does not always exist a direct noise/vibration transmission path between (or across) the internal and external transducers in the rotary compressor. The noise/vibration is thought to be primarily transmitted around the compressor shell. In other words, the primary transmission path of the rotary compressor is along the fixed medium, while that of the scroll compressor is along the time-varying medium (this is true in the relative sense since both compressors have been classified as the PLCS's/LTIS's).

(2) There exists a gap in the rotary compressor between the rotor and the shell which may act as a noise/vibration absorber, while there is no gap in the scroll compressor since the fixed scroll and the orbiting scroll are always in contact with each other.

4. Concluding Remarks

By experimental validation using a scroll compressor and a rotary compressor, a linear cyclic system is shown to 1) produce amplitude modulated input signals whose carrier frequencies are the harmonic multiples of the system's fundamental frequency, and 2) generate sideband signals whose phases are dependent upon the crank angle of the system. In addition, the sideband criterion proposed in Part I is applied to classify the scroll and rotary compressors as the PLCS's/LTIS's, which makes signal processing techniques for the LTIS's viable tools for the noise/vibration source and transmission path identification in the scroll and rotary compressors. Although restricted to the two compressors, the approach taken, in this paper may well be valid for other LCS's, e.g. the automobile engines.

Acknowledgement

The authors wish to thank Dr. Aldo Peracchio, Dr. Timothy Wagner, David Cutts, and David Young for useful discussions about the paper and technical support. This research was supported in part by a grant from the BK-21 Program for Mechanical and Aerospace Engineering Research at Seoul National University and Institute of Advanced Machinery and Design at Seoul National University.

References

Barker, R. W. and Hinich, M. J., 1994, "Statistical Monitoring of Rotating Machinery by Cumulant Spectral Analysis," in *Proc. of the SPIE*, San diego, CA, USA, Vol. 2296, pp. 43~51.

Belousov, Y. I. and Rimskii-Korsakov, A. V., 1975, "The Reciprocity Principle in Acoustics and Its Application to the Calculation of Sound Fields of Bodies," *Sov. Phys. Acoust.*, Vol. 21, No. 2, pp. 103~109.

Bradley, J. S., 1993, "Disturbance Caused by Residential air Conditioner Noise," J. Acoustic. *Soc. Am.*, Vol. 94.

Cann, R. G., 1992, "New Diagnostic Procedures for Locating Faults in Diesel Engines, "*Diesel and Gas Turbine Worldwide*, Vol. 24, No. 6, pp. 52~55.

Comparin, R. J., 1994, "Vibration Isolation for Noise Control in Residential Condensing Units," in *Proc. International Compressor Engineering Conference*, Purdue Univ., West Lafayette, IN, USA.

Faulkner, L. L., 1976, Handbook of Industrial Noise Control, Industrial Press Inc., New York, NY, USA.

Ha, H. T. R., 1995, "Vibration Control of Rotor," *KSME*, Vol. 35, No. 10, pp. 917~923, 1225~5955.

Harrap, M. J. and Wang, W. Y., 1994, "Vibration Analysis Techniques Used if Machinery fault detection," *Acoustics Australia*, Vol. 22, No. 3, pp. 91~95.

Kinsler, L. E., Frey A. R., Coppens, A. B., and Sanders, J. V., 1982, *Fundamental of Acoustics*, John Wiley & Sons, 3rd edition.

Lou, K. N., Sherman, P. J., and Lyon, D. E., 1993, "System Identification and Coherence Analysis in the Presence of a Harmonic Signal,"

Mechanical Systems and Signal Processing, vol. 7, no. 1, pp. 13~27.

Meng, Quingfeng and Qu, Liangsheng, 1991, "Rotating Machinery Fault Diagnosis Using Wigner Distribution," *Mechanical Systems and Signal Processing*, Vol. 5, No. 3, pp. 155~166.

Oh, J. Y., 1993, "The Active Noise Control in Harmonic Enclosed Sound Fields (I) : Computer Simulation," *KSME*, Vol. 17, No. 5, pp. 1054~1065, 1225~5963.

Rantala, S. and Suoranta, R., 1991, "Enhanced Vibration Monitoring Using Parametric Modelling Techniques," in *Proc. of IEEE intrumentation and Measurement Technology Conference*, Atlanta, GA, USA.

Smith, D. G., Amold, M. F., Ziegler, Jr. E. W., and Brown, M., 1992, "A Systems Approach to Appliance Compressor Quieting Using Active Noise Control Techniques," *in Proc. International Compressor Engineering Conference*, Purde Univ., West Lafayette, IN, USA.

Tamaki, K., Matsuoka, Y., Uno, M., and Kawana, T., 1995, "Wavelet Transform Based Signal Waveform Discrimination for Inspection of Rotating Machinery," *Transactions of the Institute of Electrical Engineers of Japan, Part* D, Vol. 115-D, No. 6, pp. 775~783.

Ten Wolde, T., 1973, *Reciprocity Experiments on the Transmission of Sound in Ships*, PhD thesis, Delft University.

Ten Wolde, T., 1976, "Reciprocity Measurement of Acoustical Source Strength in an Arbitrary Surrounding," *Nosie Control Engineering*, pp. 16~23.

Wagner, T. and Peracchio, A., 1996, "A Reciprocity-Based Technique for Ranking Source/Path Contribution to source Vibration and Radiated Noise," NOISE-CON 96, Bellevue, WA, USA.

Young, D. L., 1994, "Source Identification and Advanced Signal Processing Methods: User's Guide," Tech. Rep. UTRC 94-37, Advanced Compressor Technology, United Technologies Research Center, E. Hartford, CT.